IEEE Access
Multidisciplinary | Rapid Review | Open Access Journal

Received October 7, 2018, accepted November 8, 2018, date of publication November 12, 2018,
date of current version December 18, 2018.

Digital Object Identifier 10.1109/ACCESS.2018.2880989

Modeling and Analysis of a Novel Decoupled Vibration-Assisted Swing Cutting System for Micro/Nano-Machining Surface

JIEQIONG LIN[1], DONGPO ZHAO[1], MINGMING LU[1], AND ALLEN YI[2]

[1]Key Laboratory of Micro-Nano and Ultra-precision Manufacturing of Jilin Province, School of Mechatronic Engineering, Changchun University of Technology, Changchun 130012, China

[2]Department of Industrial, Welding and Systems Engineering, The Ohio State University, Columbus, OH 43210, USA

Corresponding author: Mingming Lu (lumm@ccut.edu.cn)

This work was supported in part by the Ministry of Science and Technology State Key Support Program under Grant 2016YFE0105100, in part by the Micro-Nano and Ultra-Precision Key Laboratory of Jilin Province under Grant 20140622008JC, in part by the Science and Technology Development Projects of Jilin Province under Grants 20180101034JC and 20180201052GX, and in part by the Education Department Scientific Research Planning Project of Jilin Provincial under Grant JJKH20181038KJ.

ABSTRACT The flexure-based motion platform with high-positioning precision and fast response is really attractive for the realization of micro/nano-machining surface. However, coupling motion effect existed in most positioning systems, which will induce the asymmetry and incline deformation and lead to a poor processing quality. To alleviate this problem, we proposed a decoupled vibration-assisted swing cutting (VASC) system driven by two piezoelectric actuators in this paper. A double symmetric L-shaped parallel flexure hinge with decoupled actuation and decoupled output motion has been designed in this system. In order to analyze the effect of the parameter variation to the system, the kinematics, statics, and dynamics properties of the VASC system were modeled by the geometrical method, matrix-based compliance modeling, and Lagrangian principle, respectively. Meanwhile, we have validated the effect of the parameter variation for angle-position trajectory, output stiffness, and natural frequencies by simulation analysis. In addition, the decoupled performance could be determined by finite-element analysis. In the view of the decoupling property, the result shows that the motion stroke of the input end can reach up to 15.67 μm, and the coupling ration has effectively decreased to 1.27%. Both analysis and experiment have verified the decoupled properties of VASC that have proved the effectiveness of the present VASC system for micro/nano-machining surface.

INDEX TERMS Vibration-assisted swing cutting, L-shaped flexure hinge, simulation analysis, decoupled performance, finite element analysis.

I. INTRODUCTION

In recent years, elliptical vibration cutting (EVC) technology has attracted intense attention in a widespread area of industrial appliances such as aerospace, biomedical and other fields of engineering [1]–[4]. EVC technology is regarded as one of the major methods for micro/nano-machining surface at present. It has been paid much attention due to the unique characteristics of tool-chip separation and friction reversal. However, the residual-height between adjacent trajectories caused by intrinsic attribute of EVC apparatus cannot be effectively eliminated, which limits the further improvement of machining precision. The limitation could be alleviated by increasing cutting frequency, but hysteresis effect could be appeared when the frequency was too high, which would increase the difficulty of control. To alleviate this problem, we proposed a new vibration-assisted swing cutting (VASC) system. The system has the characteristics of the pseudo-intermittent cutting and friction reversal, which has a greatly the extend tool-life and reduce cutting forces. VASC system has the characteristic of the cutting tool swing around the tool location point in machining processes, which alleviate residual-height, and improve machining accuracy effectively. Whether it is EVC or VASC, the effect of system coupling on system control stability and machining accuracy have always been the focus on the research. The solution is generally divided into structural decoupling and

control decoupling. Yao *et al.* [5] designed a decoupled XY micro-positioning platform with 4-bar mechanisms to provide decoupling. While the coupling motion was reduced to a small amount, however, the complex of the decoupling structure would lead to the system response speed more slowly. Polit and Dong [6] built a parallel and decoupled symmetric XY positioning platform, in which slender compliant parallelogram structure is utilized to obtain the decoupling effect. The bandwidth of their platform was high, but it will suffer from low load mass and poor thermal performance. Moreover, over constraint will cause stress stiffening and augment the transverse stiffness in the existence of the axial stresses [7], [8]. To overcome these disadvantages, the parallel L-shaped flexure hinges were employed in VASC system, which has a great property with high stiffness, high load carrying capacity as well as high preciseness, etc [9]. The actuation isolation and output decoupling properties of the L-shaped flexure hinges advance the use of the single-input or single-output controllers. Meanwhile, the decoupled properties were investigated by finite element analysis (FEA). Since the properties of the nano-scale displacement resolution, high-stiffness, and high-speed frequency response, the piezoelectric actuators (PZTs) were chosen as the VASC actuating device [10], [11]. To satisfy practical application of the VASC, we used decoupled L-shaped flexure hinges to make a trade-off among decoupling effect, kinematic, compliance, and dynamic performance.

The kinematic, compliance and dynamics characteristics analyses were the main elements in VASC mechanism designing. The kinematics, statics, and dynamics properties of the VASC system were modeled by the geometrical method (GM), matrix-based compliance modeling (MCM), and Lagrangian principle, respectively [12]–[15]. To analyze the effect of the parameter variation on the system, the simulation analysis was utilized, which validate the effect of the parameter variation for the angle–position trajectory, output stiffness, and natural frequency. With the parameters variation of the amplitude and angular frequency, the simulation and experimental analysis result shown that the swing motion trajectory and angle were consistent with actual result ones. Finally, the optimized structural parameters were determined by simulation analysis. According to the consistency of analysis and experiment, which have proved the effectiveness of the present VASC system for micro/nano-machining surface.

The paper is made up of the following sections: In section 2, mechanical design of a novel decoupled VASC system is proposed. In Section 3, the kinematics, compliance and dynamic modeling are established in the VASC system, and the effect of the parameters variation on the angle–position, the output stiffness and natural frequencies are simulated and analyzed in Matlab R2014a. Section 4 summarizes the decouple performance of the FEA investigation. Off-machine performance examinations of VASC are executed in section 5. The conclusions of this work are described in section 6.

II. MECHANICAL DESIGN OF VIBRATION-ASSISTED SWING CUTTING SYSTEM

In our previous work, the EVC system was developed [16]–[18]. However, EVC system generates the residual-height of the textured surfaces and seriously influences the uniformity and accuracy of the surface texture structure. Thus, this paper proposes a new VASC system. VASC system is depicted in FIGURE 1. VASC system consists of the PZT, capacitive displacement sensor probes (CDSP), capacitive displacement sensor installed pre-clamp seats (CDSIPS), capacitive displacement sensor measurement baffles (CDSMB), etc. FIGURE 1(a) and 1(d) shows the left and right 3D assembly drawings of VASC system. FIGURE 1(b) and 1(c) indicates the left and right 3D assembly drawings of VASC flexure mechanism.

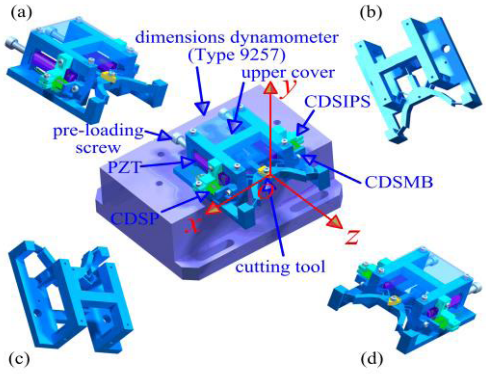

FIGURE 1. The mechanical structure of the designed VASC system.

As shown in FIGURE 2(a), the mechanism was designed symmetric by z-axis and made up of four key components: two symmetric driving units (DUs), A and B, swing motion platform unite (SMPU), and L-shaped flexure hinge guidance units (LFHGU). DU was composed of four legs, each legs was named the Leaf spring flexure hinge (LSFH) as depicted in FIGURE 2(d). The SMPU consists of three LSFH and swing motion platform (SMP) for installing the cutting tool. Meanwhile, three leaf spring flexure hinges have a 120° structures linked to SMP, as shown in FIGURE 2(b). Thus, the accuracy and stability of VASC can be ensured. LFHGU was composed of four LFHs, as indicated in FIGURE 2(c).

The fixed Cartesian coordinate system $O_{out} - u^x_{out} u^y_{out} u^z_{out}$ at the tool location point; the Cartesian coordinate system $O^L_{in} - xyz$,

$O^L - x^L y^L z^L$, and $O_i - x_i y_i z_i (i = 1, 2, 3)$ of left-DU flexure, left-LFHs flexure, and the LSFH of SMPU, respectively, as illustrated in FIGURE 2. The swing of the cutting tool was driven by the LFHGU mechanism around the y-axis, which corresponds swing principle and properties will be described in the next section.

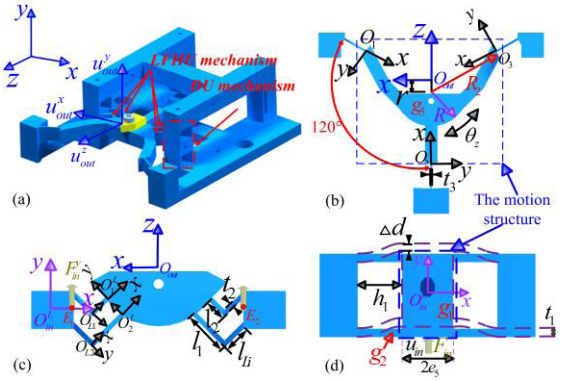

FIGURE 2. Schematic of the mechanical structure of VASC, (a) The flexure system, (b) The SMPU mechanism, (c) the LFHGU mechanism and (d) the DU mechanism.

III. MODELING AND PARAMETRIC VARIATION ANALYSIS OF VASC

A. ANALYTICAL MODELING OF VASC

1) KINEMATIC MODELING

In this section, the geometrical method (GM) was employed for the kinematics analysis in VASC system. As shown in FIGURE 3, according to GM, the LSFH and LFH can be regarded as equivalent rigid-link mechanism. A and B were driven by two PZTs, they are parallel to each other. When A and B are driven by PZTs to A_1 and B_1, the input displacement of $z_1(t)$ and $z_2(t)$, respectively. In addition, the bi-directional swing motions in z-axis were achieved by the principle of differential motion.

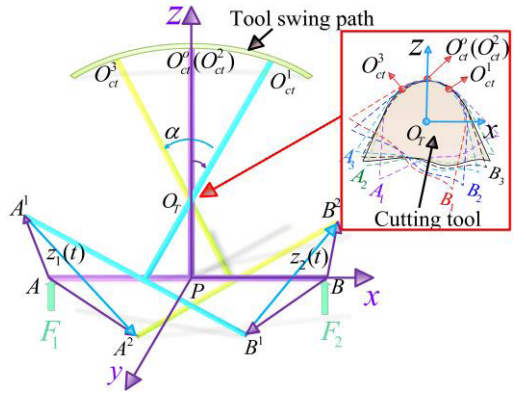

FIGURE 3. The geometrical method (GM) of VASC.

FIGURE 3 shows the joints O^1_{ct}, $O^0_{ct}(O^2_{ct})$, O^3_{ct} and O_T were located on the cutting tool, the joint A and B were distributed on DU mechanism. Owing to the overall compliance mechanism consists of the left and right symmetric at the z-axis, the left and right SMP mechanism has the unanimous structural parameters. The cutting tool point O^1_{ct}, $O^0_{ct}(O^2_{ct})$ and O^3_{ct} can be swing around the center of SMP mechanism (the tool location point), O_T. Therefore, the motion joints O^1_{ct}, $O^0_{ct}(O^2_{ct})$ and O^3_{ct} can be confined to the circular surface, as illustrated in FIGURE 4.

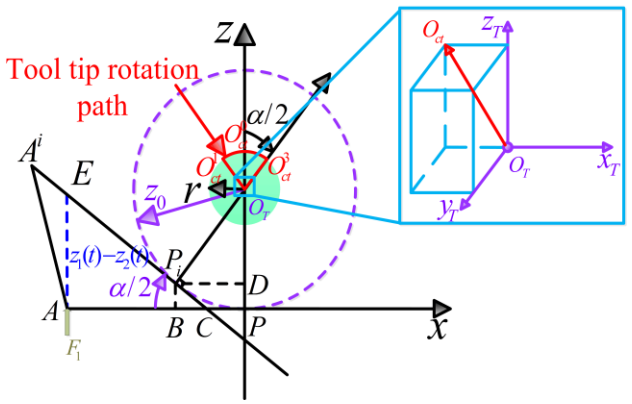

FIGURE 4. The GM of the output platform: After the swing adjustments.

In VASC, the two PZTs input signals can be described as

$$\begin{cases} X_1(t) = A1\cos(w_1 t + \varphi_1) \\ X_2(t) = A2\cos(w_2 t + \varphi_2) \end{cases} \tag{1}$$

Where, $A1$ and $A2$ represents the input single amplitude of two PZTs, respectively; w_1, φ_1 and w_2, φ_2 are the input single angular frequency and phase of two PZTs, respectively, and $w_1 = w_2$; t is the input signals time.

To purpose of the angle-position trajectory analysis, as indicated in FIGURE 4, we assign the fixed Cartesian coordinate system $O_T - x_T y_T z_T$ at the center of SMP mechanism, O_T, the joints O^1_{ct}, $O^0_{ct}(O^2_{ct})$ and O^3_{ct} with the circumcircle radius of r. To be simple without losing generality, two PZTs are installed parallel to thez_T-axis, y_T is perpendicular to the tool rake face.

The output displacement of work-piece and tool-tip point were generated by two PZTs in the Cartesian coordinate system, can be represented as follow

$$\begin{cases} z_1(t) = A3\cos(w_3 t + \psi_1) \\ z_2(t) = A4\cos(w_4 t + \psi_2) \end{cases} \tag{2}$$

Where, $A3$ and V_4 represents the amplitudes of the tool-tip point output displacement by two PZTs, respectively; w_3, ψ_1 and w_4, ψ_2 represent the angular frequency and phase in the driving signals along $z_1(t)$ and $z_2(t)$ directions, respectively, and $w_3 = w_4$.

When the initial phases ψ_1 and ψ_2 are adjusted by two PZTs, respectively. We have

$$\psi_1 - \psi_2 = \theta \tag{3}$$

Where θ is a constant. Hence, from Eq. (3) we can get

$$\begin{cases} z_1(t) = A3\cos(w_3 t + \theta) \\ z_2(t) = A4\cos(w_4 t) \end{cases} \tag{4}$$

Assume the tool location point, O_T, of the coordinate is (0, 0, z_0), and the swing motion angle of α. The cutting tool swing motion radius of r. $AB = 2l_0$, $2l_0$ is the displacement of the two PZTs at x-axis direction. The coordinate point of P_i is set

to $(x_i, 0, z_i)$, and the point at the flexure hinge platform can be described as:

$$\begin{cases} x_i = P_iD = O_TP_i\sin(\alpha/2) = z_0\sin(\alpha/2) \\ z_i = P_iB = z_0 - O_TP_i\cos(\alpha/2) = z_0 - z_0\cos(\alpha/2) \end{cases} \tag{5}$$

Where $z_0 = P_iO_T$ and $\angle P_iCB = \alpha/2$, with

$$\begin{cases} BC = P_iB/\tan(\alpha/2) \\ PC = x_i - BC = z_0\sin(\alpha/2) \\ \quad -(z_0 - z_0\cos(\alpha/2))/\tan(\alpha/2) \\ AC = l_0 - PC = l_0 - z_0\sin(\alpha/2) \\ \quad +(z_0 - z_0\cos(\alpha/2))/\tan(\alpha/2) \end{cases} \tag{6}$$

As indicated in FIGURE 4, due to $P_iCB \cong ECA$, which is given as

$$\begin{aligned} \frac{P_iB}{EA} &= \frac{BC}{AC} = \frac{z_0 - z_0\cos(\alpha/2)}{z_1(t) - z_2(t)} \\ &= \frac{(z_0 - z_0\cos(\alpha/2))/\tan(\alpha/2)}{l_0 - z_0\sin(\alpha/2) + (z_0 - z_0\cos(\alpha/2))/\tan(\alpha/2)} \end{aligned} \tag{7}$$

With

$$l_0\sin(\alpha/2) - (z_1(t) - z_2(t) - z_0)\cos(\alpha/2) = z_0 \tag{8}$$

Through theoretical calculations, the swing motion angle of tool on the flexure hinge platform can be described as:

$$\begin{aligned} \alpha = {} & 2\arccos\left(\frac{z_0}{\sqrt{l_0^2 + (z_1(t) - z_2(t) - z_0)^2}}\right) \\ & + 2\arctan\frac{l_0}{\sqrt{l_0 + (z_1(t) - z_2(t) - z_0)}} \end{aligned} \tag{9}$$

To purpose of the swing motion trajectory analysis, we assign a motion Cartesian coordinate system $P_i - x_iy_iz_i$ at the point P_i(i = 0, 1, 2…n), from Eq. (9) we can get

$$\begin{cases} x_i = z_0\sin\frac{\alpha}{2} \\ y_i = 0 \\ z_i = z_0 - z_0\cos\frac{\alpha}{2} \end{cases} \tag{10}$$

By the mathematical geometry, the swing path around the cutting tool location point, O_T, can be described as

$$\begin{cases} x_{ct} = x_ir/z_0 \\ y_{ct} = 0 \\ z_i/z_{ct} = (z_i/\cos(\alpha/2))/(z_0 - r\cos(\alpha/2)) \end{cases} \tag{11}$$

According to Eq. (10) and (11), the trajectory of swing motion can be obtained as follows

$$\begin{cases} x_{ct} = (z_0\sin\frac{\alpha}{2}) \times r/z_0 \\ y_{ct} = 0 \\ z_{ct} = (z_0 - r\cos(\alpha/2))\cos(\alpha/2) \end{cases} \tag{12}$$

Hence, swing motion trajectory of the cutting tool is described as

$$(r\sin\frac{\alpha}{2})^2 + ((z_0 - r\cos(\alpha/2))\cos(\alpha/2) + z_0)^2 = z_0^2 \tag{13}$$

According to Eq. (3), the phase difference θ was generated by PZTs. Thus, the swing motion trajectory of tool-tip can be generated in 2D space. Meanwhile, $A3, A4, w_3, w_4$ and θ were actively adjusted by the two signal, $z_1(t)$ and $z_2(t)$. The cutting tool could be independent achieved control parameters by the swing motion, to adapt to different cutting condition.

2) COMPLIANCE MODELING

To establish the compliance model of the VASC, the local compliances need to be transformed into a global frame selected to describe the mechanism. Then, the stiffness connected in parallel compliances connected in serial and can be, respectively, extra together to generate the whole model of the flexure mechanism. In this section, the output and input of compliance properties are given according to MCM [19], [20].

The output compliance of the LFHGU mechanism as

$$C_{out}^{LU} = [(C_L^{LU})^{-1} + (T_{\mathrm{rz}}(\pi)C_L^{LU}(T_{\mathrm{rz}}(\pi))^T)^{-1}]^{-1} \tag{14}$$

where $T_{rz}(\pi)$ is the coordinate transform matrix around the z-axis by an angle of π. C_L^{LU} is the output compliance of the left-half chain of the DU and LFHGU mechanism.

Since the relationship between each LSFH is considered, the output compliance of the RMP mechanism relative to the fixed base as

$$C_{O_{out}}^{M} = [(C_{L1}^{O_{out}})^{-1} + (C_{L2}^{O_{out}})^{-1} + (C_{L3}^{O_{out}})^{-1}]^{-1} \tag{15}$$

Where $C_{Li}^{O_{out}}(i = 1, 2, 3)$ represents the frame $M_{Li}(i = 1, 2, 3)$ may be transformed to the reference frame O_{out}.

Thus, the overall VASC system flexure mechanism consists of the DUs, LFHGU, and LSFHs connected in parallel manners on SMP. Thus, the output compliance of VASC system is given by

$$\begin{aligned} C_{out}^{all} &= [(C_L^{LU})^{-1} + (T_{\mathrm{rz}}(\pi)C_L^{LU}(T_{\mathrm{rz}}(\pi))^T)^{-1} \\ &\quad + (C_{L1}^{O_{out}})^{-1} + (C_{L2}^{O_{out}})^{-1} + (C_{L3}^{O_{out}})^{-1}]^{-1} \\ &= diag(C_{\delta_x,F_x}, C_{\delta_y,F_y}, C_{\delta_z,F_z}, C_{\theta_x,M_x}, C_{\theta_y,M_y}, C_{\theta_z,M_z}) \end{aligned} \tag{16}$$

Where, C_L^{LU} represents the output compliance of the left-half chain of the DU and LFHGU mechanism, $T_{rz}(\pi)$ is the coordinate transform matrix around the z-axis by an angle of π, $C_{L1}^{O_{out}}$, $C_{L2}^{O_{out}}$, and $C_{L3}^{O_{out}}$ represent the output compliance of each LSFH on SMP.

3) DYNAMICS MODELING

To describe the free vibration of VASC, the displacements at the two input ends $d = [z_1, z_2]^T$ are defined as the generalized coordinate variable. Therefore, the total kinetic energy of system can be given by

$$\begin{aligned} T = {} & \frac{1}{2}\cdot[4\cdot I[(\frac{\dot{z}_1}{h_1})^2 + (\frac{\dot{z}_2}{h_1})^2] + (m_{g_1} + m_{g3_1} + m_{g3_2}) \\ & \bullet[\dot{z}_1^2 + \dot{z}_2^2] + (3\cdot m_{g4} + m_{g5})\left[\dot{z}^2 + \dot{x}^2\right]] \end{aligned} \tag{17}$$

Where, x and z are the fixed Cartesian coordinate on the system O-$xyz$of the radius R_2; m_{g31}, m_{g32}, m_{g4} and m_{g5} denotes mass of the system of the top LFH, the down LFH, the three positioning LSFHs and the SMP, respectively.

We are able to obtain potential energy as

$$V = \frac{\dot{z}_1^2}{2 \bullet C_{\delta_z,F_z}} + \frac{\dot{z}_2^2}{2 \bullet C_{\delta_z,F_z}} \tag{18}$$

The Lagrange equation is used in VASC system, in which the damping effect is neglected. Thus, substituting T into Lagrange's equation [12]:

$$\frac{d}{dt}(\frac{\partial T}{\partial \dot{d}}) + \frac{\partial V}{\partial d} - \frac{\partial T}{\partial d} = F \tag{19}$$

Hence, through solving the equation of dynamics properties, the natural frequencies can be calculated as

$$f_1 = \frac{1}{2\pi}\sqrt{K_{in}\frac{M_1 - M_2}{M_1^2 - M_2^2}}$$
$$f_2 = \frac{1}{2\pi}\sqrt{K_{in}\frac{M_1 + M_2}{M_1^2 - M_2^2}} \tag{20}$$

Where M_1 and M_2 equivalent quality matrix, and K_{in} is the input stiffness of the VASC.

B. PARAMETERS ANALYSIS OF VASC

1) THE EFFECT OF THE PARAMETERS VARIATION OF THE ANGLE-POSITION TRAJECTORY

In view of Eqs.(9) and (12), the calculation modeling of cutting tool was simulated by Matlab R2014a. The phase difference $\theta = \pi$ was adopted in VASC. According to **TABLE 1**, the variation trajectory of the cutting tool-tip could be received, as illustrated in FIGURE 5(a). Meanwhile, the variation swing motion angle of the cutting tool-tip could be received, which is indicated in FIGURE 5 (b).

TABLE 1. Generate parameters for the angle-position trajectories.

	Displacement l_0 (mm)	Amplitude A (μm)		Angular frequency W (Hz)	
		$A3$	$A4$	w_3	w_4
I	22.5	4	4	50	50
II	22.5	4	4	100	100
III	22.5	3	3	50	50
IV	25	4	4	50	50

As shown in FIGURE 5, with adjusting the relevant parameters, the swing trajectory and angle of cutting tool-tip can be changed flexibly. Basing on the trajectory I as the benchmark, when the change of the angular frequency of two PZTs in the trajectory II, which space and angle size of the swing trajectory of the tool can not be changed, but the rotation cycle of the tool trajectory had faster. In the trajectory III, with changing the amplitude of two PZTs, space and angle size of the swing trajectory of the tool was changed. In the trajectory IV, with changing the position of two PZTs, not only the space and angle size of the swing motion trajectory can be changed, but also space and angle size of the swing trajectory of the tool are greater than III. Thus, by adjusting the relevant parameters of the system, a better the swinging trajectory and angle of cutting tool-tip can be achieved, which is the advantage of reducing average cutting force, extending tool-life, and improving machining quality so on.

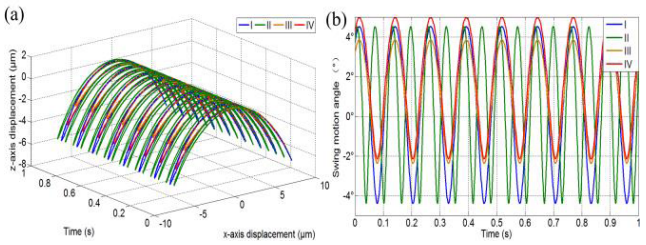

FIGURE 5. The effect of the parameters variation of the angle – position trajectory, (a) effect of the swing trajectory with parameter variation, and (b) effect of the swing motion angle with parameter variation.

2) THE EFFECT OF THE PARAMETERS VARIATION OF OUTPUT STIFFNESS AND NATURAL FREQUENCIES TRAJECTORY

The output stiffness and natural frequency model of VASC structure affected by the parameters in three aspects. The parameters of the flexure hinges:t_1, h_1, b_1, t_2, $l_{Li}(i = 1, 2)$, l_1, l_2, t_3; the parameters of the motion structure: R_2, e_5; and the parameters of structure material: E, ρ. In the design process, the material of the spring steel was employed in VASC, which the material properties are as follows: Poisson ration, $\mu = 0.3$; Density, $\rho = 7.85 \times 10^3 kg/m^3$; Young's Modulus, $E = 2.06 \times 10^{11} pa$.

To improve the performance of VASC, we have achieved analyze of the parameter variation for the output stiffness and natural frequency by simulation analysis. The variation of each parameter had different influence in the compliance and dynamics modeling. Thus, the effect of the parameter variation for the output stiffness and natural frequencies were given in FIGURE 6. FIGURE 6 (a) and (b) illustrate the parameter variation of the natural frequency and output stiffness on the flexure hinges, which the range of the parameter values were given as: $t_1, t_2, t_3 \in [0.5, 1.5]$, with the variation of DU flexure hinge thickness t_1 (Set:$t_2 = 1, t_3 = 1.2$), the natural frequency and output stiffness almost do not change; when the variation of LFHGU flexure hinge thickness $0.5 \leq t_2 \leq 1.5$(Set:$t_1 = 1, t_3 = 1.2$), the natural frequency reduces greatly along the rise of the thickness t_2, the output stiffness increases with the rise of thickness t_2, z-axis was faster than x-axis; with the variation of SMPU flexure hinges thickness $0.5 \leq t_3 \leq 1.5$ (Set:$t_1 = 1, t_2 = 1$), the natural frequency reduces along with the rise of thickness t_3 and natural frequency was fall faster, which the change of output stiffness was the same along the x-axis and z-axis directions. As indicated in FIGURE 6 (c) and (d),

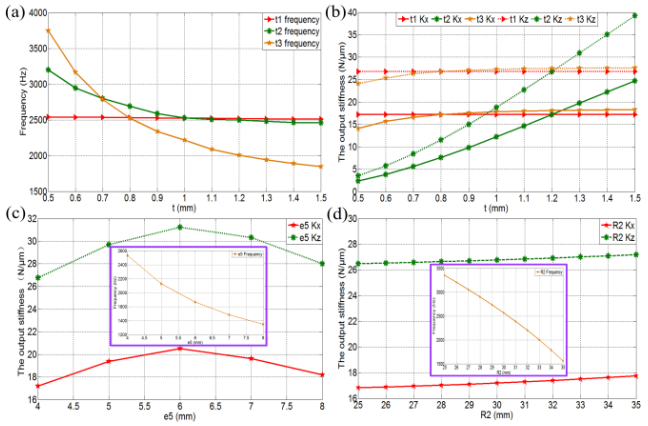

FIGURE 6. The effect of the parameters variation of the stiffness and frequencies trajectory, (a) the corresponding natural frequency in terms of structure parameters t_1, t_2 and t_3, respectively; (b) the corresponding the output stiffness in terms of structure parameters t_1, t_2 and t_3, respectively; (c) and (d) the corresponding the natural frequency and the output stiffness in terms of structure parameters e_5 and R_2, respectively.

the parameter variation of the natural frequency and output stiffness on the motion structure, which the range of each parameter value gives as: $e_5 \in [4, 8]$ and $R_2 \in [25, 35]$, with the increase of the motion structure e_5(Set:$R_2 = 30$), which the natural frequency was reduced greatly, the output stiffness was rise first, and then falls. When R_2 was larger than 25mm and smaller than 35mm (Set:$e_5 = 4$), the natural frequency of the motion structure decreases greatly with the raise of R_2, and the output stiffness increases along rise of R_2.

According to parameters analysis, (1) in Eq. (13), with the change of the angular frequency, the space and angle size of the swing trajectory could not be changed, but the change the control amplitude and signals position of the swing trajectory could be changed; (2)the output stiffness, and natural frequency were calculated by Eq. (16), and (20), respectively. which the compliance of the x- and z-axis direction are 0.0581μm/N and 0.0373μm/N, respectively, the first two natural frequencies are 2558.6Hz and 3342.1Hz, which was the working bandwidth of VASC. Meanwhile, the output stiffness and natural frequency analytical has been verified through FEA and experiments in [20]. As shown in FIGURE 2, the structure parameter values were listed in TABLE 2:

IV. DECOUPLING PERFORMANCE INVESTIGATION OF THE FEA IN VASC

In order to evaluate the established analysis model, decoupling performance analysis of VASC mechanism based on FEA was carried out by ANSYS Workbench 16.0 platforms. The output decoupling indicates that it does not generate motions in other directions when platform motions along one specified direction; the input decoupling means that an actuator will not be damaged by the motions of the other actuators [21].

TABLE 2. Structure parameter of system. (Unit: mm)

t_1	t_2	t_3	e_5	R_2	h_1	b_1	l_{Li}	l_1	l_2
0.9	1	0.6	4	30	7.1	10	6.3	5.1	10.5

In order to the decoupling performance, two sequences along z1-axis and z2-axis input forces with constant summations or differences were used. Based on the FEA, to obtain the coupled motion component generated by the mechanism motion along the z_{out}-axis on the x_{out}-axis, the constant driving force sums were applied to two driving ends, and the obtained two-axis motion as indicated in FIGURE 7 (a). To obtain the coupled motion component generated by the mechanism motion along the x_{out}-axis on the z_{out}-axis, the constant driving force differences were applied to the two driving ends, and the obtained two-axis motion as illustrated in FIGURE 7 (b). FIGURE 7 indicates the linear relation between the driving force and motion displacement in x_{out} −direction and z_{out} −direction. Furthermore, the induced coupling motions along u^x_{out} and u^z_{out} directions were 7.5nm and 4.4nm, respectively. In the whole range of motion, the coupling motions were less than 0.18%, which were negligible. Thus, the output decoupling is significantly improved in VASC mechanism.

In the input coupling of VASC, the motion along the driving direction can be resisted by the actuator or the preloads of the flexural mechanism, without negatively affecting the PZTs. However, the lateral motions will introduce shear impacts on the PZTs, which will cause damage to PZTs [21]. To investigate the isolation performance, using FEA to calculate the lateral motion at the middle point of the two interfaces (the rigid body, g_1).

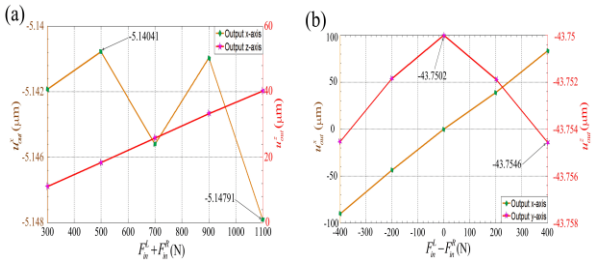

FIGURE 7. Output moving features of the mechanism: (a) sum of the forces and (b) difference of the forces. u^x_{out} and u^z_{out} correspond to the lines with diamond and five-pointed star.

The input coupling motion is in direct proportion to the summation of the z1-axis and z2-axis driving forces. According to the output motions, the input coupling along the x_{in}-axis (the motion of DU mechanism) motions was 1.25%. Conversely, the lateral motions have no relation with the difference of the driving force, which indicate that the motion along z_{in}-axis (the motion of DU mechanism) will be no lateral movement at the input end. Compared with the report in [21] and [22], the decoupling performance of the system has been significantly improved.

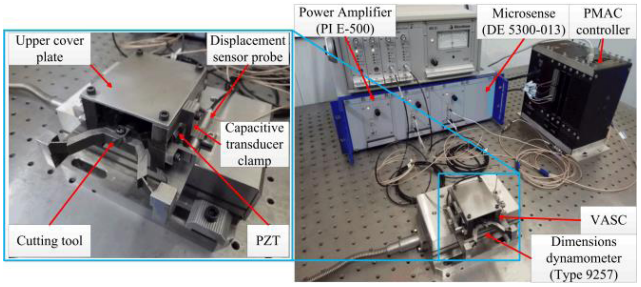

FIGURE 8. Schematic of the experimental apparatus setup.

V. EXPERIMENTAL TESTING OF VASC MECHANISM

The configuration for performance testing of the proposed system is illustrated in FIGURE 8. VASC mechanism is actuated by two Parallel PZTs (40VS12, Harbin). The Power PMAC (Delta Tau Inc) is employed to generate a test signal. The test signal is amplified by the Power Amplifier (E-500, PI Inc.). Then PZTs are sued to realize the vibration. The capacitive transducer (Modem 5300, microsence Inc.) with four measuring channels is used to measure the dynamic displacement, and closed-loop control is formed as a feedback signal. The wide range of PID control algorithm is selected to form the closed loop control system. In order to decrease the interference outside itself, the tests are performed on a vibration-isolated air bearing platform. The system total noise value of the z1-axis and z2-axis testing channel are about 35.14nm and 38.02nm, respectively.

A. SINE RESPONSE TESTS

In this paper, the developed apparatus was tested by the sinusoidal signal response. Sinusoidal excitations were applied along with the z1- and z2-axis, as illustrated in FIGURE 9. FIGURE 9(a) and (b) shows the sinusoidal tracking curve along z1- and z2-axis, respectively; the sinusoidal tracking errors along the z1- and the z2-axis are also shown, respectively. FIGURE 9 shows the responses maintain good

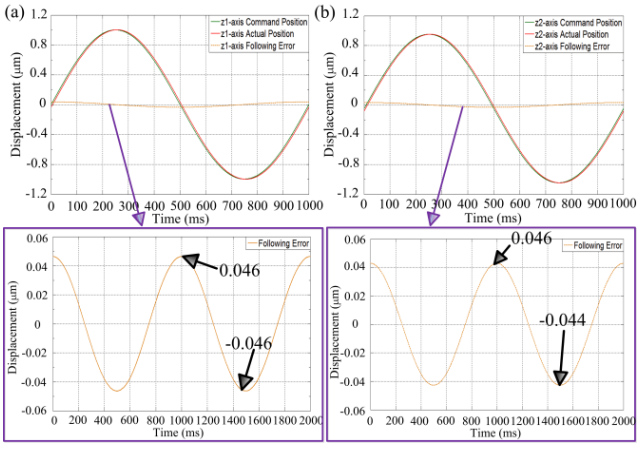

FIGURE 9. Response of the VASC system with sinusoidal tracking excitation, (a) response along the z1-axis, (b) response along the z2-axis.

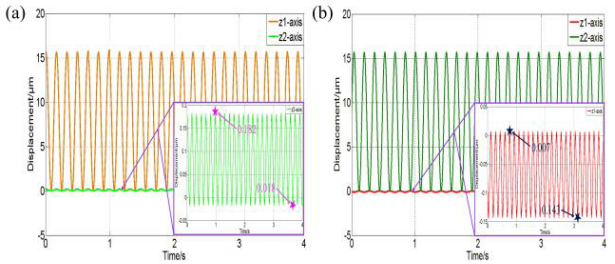

FIGURE 10. Displacement of the VASC with unidirectional actuation force, a(1) and a(2) the corresponding parasitic motions of z1-axis and z2-axis, respectively, a(3) motion along the z1-axis direction Following error, and b(1) and b(2) are the corresponding parasitic motions of z2-axis and z1-axis, respectively, b(3) motion along the z2-axis direction Following error.

sinusoidal waveforms and work stably under sinusoidal signal excitation, which is driven by two PZTs. Unfortunately, it shows a significant phase lag, but there is only a small amount of oscillation at the upper and lower ends. The practical displacement is consistent with the command displacement excellently. The maximum error is about 46nm, less than 4.35% of the whole stroke, therefore, to meet the requirements.

B. SINE STROKE AND DECOUPLING TESTS

In order to test the system stroke and decoupling property, the PZT was actuated by only one-axis, which the other-axis had not actuated by PZT. FIGURE 10(a) illustrates the z1-axis was actuated only, the input stroke, 15.67μm, the parasitic motion of the z2-axis, 0.2μm, which was about 1.27% of the input displacement in z1-axis. Similarly, FIGURE 10(b) indicates the parasitic motion of the z2-axis, 0.15μm, which was about 0.975% of the z2-axis input displacement. Basing on the theory, the bi-directional motions should symmetric, it was however, the asymmetric motion of the most approximately 0.8μm, which the inconsistent preload of two PZTs or the asymmetric structure aroused by manufacturing error. Therefore, the result shows that the decoupling design is much effective.

C. DYNAMICS PERFORMANCE TESTS

To test the dynamic characteristic, the frequency response was carried out by the sweep-frequency excitation method. FIGURE 11 illustrates the measured response of frequency, which z1- and z2-axis are approximately 1900Hz, 2686Hz and 1893Hz, 2594Hz, respectively. Practical working bandwidth is about 1000Hz. It was noteworthy that both natural frequencies were much lower than the corresponding values obtained by theoretical analysis. This phenomenon was mainly caused by the assemblage of PZTs, which could reduce the stiffness of the whole compliant system. Compared with the theoretical results, the practical and theoretical natural frequencies ratio was about 34.7%, 24.4%, which might be imperfect contacts and machining errors effect.

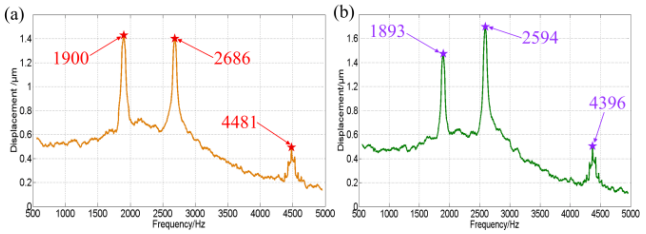

FIGURE 11. Response of the VASC system with swept excitation, (a) response along z1-axis, (b) response along z2-axis.

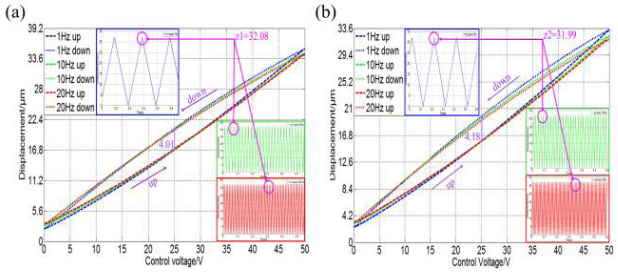

FIGURE 12. Responses of the VASC system hysteresis tests, (a) the z1-axis hysteresis tests; (b) the z2-axis hysteresis tests.

D. HYSTERESIS ANALYSIS

To survey the hysteresis of the VASC system, the triangle voltage of the amplitude, 5V, the natural frequencies of 1Hz, 10H, 20Hz, were produced by the signal generator. FIGURE 12 indicates the response of the input signal and the associated input voltage displacement, the lower and upper curve represents expansion and contraction of PZT, respectively. When the triangle voltage was 5V, the displacements along z1-axis and z2-axis can be up to 32.08μm and 31.99μm, respectively. When the frequencies input single was set to 1Hz, 10Hz and 20Hz, respectively, the maximum hysteresis displacements along z1- and z2-axis were measured of 4.01μm and 4.18μm. Thus, the hysteresis percentages of z1-axis and z2-axis were correspondingly calculated as 12.5% and 13.1%. Based on the above analysis, we need adopt appropriate control strategy to lower the hysteresis phenomenon in the future work.

E. ANALYSIS OF VASC SYSTEM ANGLE-POSITION MODEL

Due to the deliberate design of VASC structure, which was generated arbitrary vibration-assisted swing motion in 2D space. To investigate angle–position trajectory of diamond tool, the amplitude and angular frequency of the two input signals were adopted for 4μm, 4μm, 3μm and 50Hz, 100Hz, 50Hz, respectively. The input displacement of VASC system as illustrated in FIGURE 13(a). As shown in FIGURE 13(b), actuated motion trajectory of cutting tool was alone the tool location point swing back and forth. When the SMP mechanism was driven by one PZT, the cutting tool swing angle rang of 0° to 5°33', 0° to 5° 31' and 0° to 4°2', respectively. The changed of angle–position trajectory result shows that practice was consistent with the theoretical. Thus, the swing

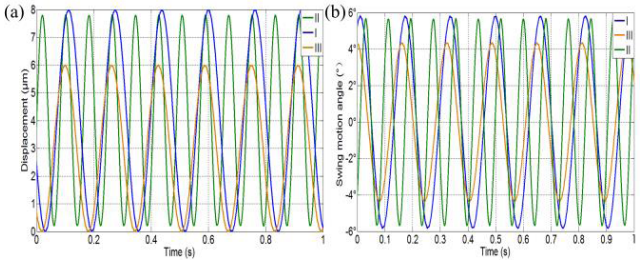

FIGURE 13. Responses of the VASC system amplitude and angular frequency parametric variation input signals, (a) the input displacement changes, and (b) the SMP rotating angle range.

trajectory and angle of cutting tool-tip could be achieved, which was the advantage of reducing average cutting force, extending tool-life, and improving machining quality so on.

VI. CONCLUSIONS

The paper presented the modeling and analysis of a novel decoupled VASC system for micro/nano-machining surface. And the using of L-shaped flexure hinge had alleviated the input and output decoupling properties. While the parameters variation of the Kinematic, compliance, and dynamic modeling are analyzed by simulation, respectively. Then the decoupling property was analyzed by FEA. Finally, according to the experimental results, the primary conclusions of the paper could be summarized as:

REFERENCES

[1] L. Jieqiong, L. Yingchun, and Z. Xiaoqin, "Tool path generation for fabricating optical freeform surfaces by non-resonant three-dimensional elliptical vibration cutting," *Proc. Inst. Mech. Eng., C, J. Mech. Eng. Sci.*, vol. 228, no. 7, pp. 1208–1222, 2014, doi: 10.1177/095440 6213502448.

[2] W.-L. Zhu, Y. He, K. F. Ehmann, Z. Zhu, and B.-F. Ju, "Modeling of the effects of phase shift on cutting performance in elliptical vibration cutting," *Int. J. Adv. Manuf. Technol.*, vol. 92, nos. 9–12, pp. 3103–3115, 2017, doi: 10.1007/s00170-017-0366-2.

[3] N. Suzuki, M. Haritani, J. Yang, R. Hino, and E. Shamoto, "Elliptical vibration cutting of tungsten alloy molds for optical glass parts," *CIRP Ann.*, vol. 56, no. 1, pp. 127–130, 2007, doi: 10.1016/j.cirp.2007.05.032.

[4] P. Guo and K. F. Ehmann, "An analysis of the surface generation mechanics of the elliptical vibration texturing process," *Int. J. Mach. Tools Manuf.*, vol. 64, pp. 85–95, Jan. 2013, doi: 10.1016/j.ijmachtools.2012.08.003.

[5] Q. Yao, J. Dong, and P. M. Ferreira, "Design analysis, fabrication and testing of a parallel-kinematic micropositioning XY stage," *Int. J. Mach. Tools Manuf.*, vol. 47, no. 6, pp. 946–961, 2007, doi: 10.1016/j.ijmachtools.2006.07.007.

[6] S. Polit and J. Dong, "Development of a high-bandwidth XY nanopositioning stage for high-rate micro-/nanomanufacturing," *IEEE/ASME Trans. Mechatron.*, vol. 16, no. 4, pp. 724–733, Aug. 2011, doi: 10.1109/tmech.2010.2052107.

[7] J. Ryu, S.-S. Kim, and S.-S. Kim, "A criterion on inclusion of stress stiffening effects in flexible multibody dynamic system simulation," *Comput. Struct.*, vol. 62, no. 6, pp. 1035–1048, 1997, doi: 10.1016/s0045-7949(96)00285-4.

[8] Q. Xu and Y. Li, "Structure Improvement of an XY flexure micromanipulator for micro/nano scale manipulation," *IFAC Proc. Volumes*, vol. 41, no. 2, pp. 12733–12738, 2008, doi: 10.3182/20080706-5-KR-1001.02154.

[9] J. P. Merlet, *Parallel Robots*. London, U.K.: Kluwer, 2000.

[10] K. K. Leang and S. Devasia, "Feedback-linearized inverse feedforward for creep, hysteresis, and vibration compensation in AFM piezoactuators," *IEEE Trans. Control Syst. Technol.*, vol. 15, no. 5, pp. 927–935, Sep. 2007, doi: 10.1109/TCST.2007.902956.

[11] G. Song, J. Zhao, X. Zhou, and J. A. De Abreu-Garcia, "Tracking control of a piezoceramic actuator with hysteresis compensation using inverse Preisach model," *IEEE/ASME Trans. Mechatronics*, vol. 10, no. 2, pp. 198–209, Apr. 2005, doi: 10.1109/tmech. 2005.844708.
[12] Z. Zhu, S. To, K. F. Ehmann, and X. Zhou, "Design, analysis, and realization of a novel piezoelectrically actuated rotary spatial vibration system for micro-/nanomachining," *IEEE/ASME Trans. Mechatronics*, vol. 22, no. 3, pp. 1227–1237, Jun. 2017, doi: 10.1109/TMECH.2017.2682983.
[13] Y. Li and Q. Xu, "Modeling and performance evaluation of a flexure-based XY parallel micromanipulator," *Mech. Mach. Theory*, vol. 44, no. 12, pp. 2127–2152, 2009, doi: 10.1016/j.mechmachtheory.2009.06.002.
[14] S. Xiao, Y. Li, and X. Zhao, "Design and analysis of a novel micro-gripper with completely parallel movement of gripping arms," in *Proc. 6th IEEE Conf. Ind. Electron. Appl. (ICIEA)*, Jun. 2011, pp. 2127–2132, doi: 10.1109/ICIEA.2011.597 5943.
[15] W.-L. Zhu, Z. Zhu, Y. He, K. F. Ehmann, B.-F. Ju, and S. Li, "Development of a novel 2-D vibration-assisted compliant cutting system for surface texturing," *IEEE/ASME Trans. Mechatronics*, vol. 22, no. 4, pp. 1796–1806, Aug. 2017, doi: 10.1109/TMECH.2017.2693996.
[16] M. Lu, J. Zhou, J. Lin, Y. Gu, J. Han, and D. Zhao, "Study on Ti-6Al-4V alloy machining applying the non-resonant three-dimensional elliptical vibration cutting," *Micromachines*, vol. 8, no. 10, p. 306, 2017, doi: 10.3390/mi8100306.
[17] M. Lu, X. Zhou, and J. Lin, "Improved memetic algorithm for nonlinear identification of a three-dimensional elliptical vibration cutting system," *Proc. Inst. Mech. Eng., I, J. Syst. Control Eng.*, vol. 228, no. 7, pp. 449–460, 2014, doi: 10.1177/0959651814530276.
[18] J. Lin, X. Jing, M. Lu, Y. Gu, and J. Han, "Study on the tool wear of 3-D elliptical vibration cutting," *Mech. Sci.*, vol. 8, no. 2, pp. 215–220, 2017, doi: 10.5194/ms-8-215-2017.
[19] Y. Li and Q. Xu, "Design and analysis of a totally decoupled flexure-based XY parallel micromanipulator," *IEEE Trans. Robot.*, vol. 25, no. 3, pp. 645–657, Jun. 2009, doi: 10.1109/tro.2009. 2014130.
[20] M. Lu *et al.*, "Design and analysis of a novel piezoelectrically actuated vibration assisted rotation cutting system," *Smart Mater. Struct.*, vol. 27, no. 9, p. 095020, 2018, doi: 10.1088/1361-665X/aad5ae.
[21] Z. Zhu, X. Zhou, Z. Liu, R. Wang, and L. Zhu, "Development of a piezoelectrically actuated two-degree-of-freedom fast tool servo with decoupled motions for micro-/nanomachining," *Precis. Eng.*, vol. 38, no. 4, pp. 809–820, 2014, doi: 10.1016/j.precisioneng.2014.04.009.
[22] H. Tang and Y. Li, "Design, analysis, and test of a novel 2-DOF nanopositioning system driven by dual mode," *IEEE Trans. Robot.*, vo. 29, no. 3, pp. 650–662, 2013, doi: 10.1109/TRO.2013.2248536.

JIEQIONG LIN received the M.Phil. degree in mechanical manufacturing from the Jilin Institute of Technology in 2001 and the Ph.D. degree in mechanical manufacturing from Jilin University, Changchun, China, in 2005.

She is currently a Professor an Associate Professor with the School of Mechatronic Engineering, Changchun University of Technology. She is an active Researcher who focuses on industry-related and applied research in ultra-precision machining, large-area laser processing, precision polishing, and error compensation.

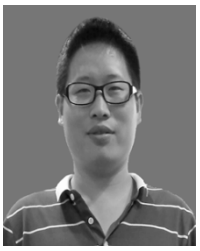

DONGPO ZHAO was born in Luohe, China, in 1990. He received the B.E. degree in mechanical engineering from Changchun Sci-Tech University in 2016. He is currently pursuing the M.E. degree with the Changchun University of Technology. His research interests include design, modeling, and control of mechatronic systems, ultra-precision diamond machining of freeform surfaces, and *in-situ* measurement.

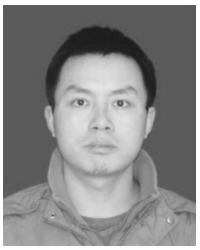

MINGMING LU received the Ph.D. degree in mechanical manufacturing from the Jilin University of Technology, Changchun, China, in 2014. He is currently an Associate Professor with the School of Mechatronic Engineering, Changchun University of Technology. His research interests are focused on 3-D elliptical vibration-assisted cutting, vibration-assisted swing cutting, micro/nano-positioning of cutting tool, and modeling and control of ultra-precision cutting.

ALLEN YI received the degree from the University of Science and Technology of China in 1986 and the Ph.D. degree from Boston University in 1993. He was with Corning Precision Lens for 10 years. In 2002, he joined The Ohio State University, where he is currently a Professor of industrial and systems engineering. He is a long-time member of the American Society for Precision Engineering.

He has authored or co-authored more than 100 technical papers in precision engineering. His research activities are in the general area of precision engineering with a focus in high volume optical fabrication, freeform, and micro-optics fabrication as well as micromachining processes for optical, medical, and biomedical device fabrication.